Invited Paper

Generation of structured beams in large-Fresnel number degenerate cavities and beam transformation with orbital angular momentum

T. H. Lu*[a], Y. C. Lin[b], Y. F. Chen[b], and K. F. Huang[b]
[a] Department of Physics, National Taiwan Normal University, Taipei, Taiwan
[b] Department of Electrophysics, National Chiao Tung University, Hsinchu, Taiwan

ABSTRACT

We employ a large-Fresnel-number laser system to demonstrate the three-dimensional optical coherent waves localized on Lissajous and trochoidal parametric surfaces with Lissajous and trochoidal transverse patterns in degenerate cavities. The coherent structured beams are verified to be composed of degenerate Hermite-Gaussian and Laguerre-Gaussian modes with different longitudinal indices resulted from longitudinal-transverse coupling. As well known, the Hermite-Gaussian modes can be converted into Laguerre-Gaussian modes possessing orbital angular momentum by use of a pair of cylindrical lens. Consequently, we make use of cylindrical lenses to transform the Lissajous structured beams superposed of degenerate Hermite-Gaussian modes into the intriguing trochoidal structured beam possessing optical orbital angular momentum.

Keywords: degenerate cavity, coherent waves, optical angular momentum

1. Introduction

In recent years, various laser systems are widely employed to realize optical transverse pattern formation including the high order Laguerre-Gaussian modes, Hermite-Gaussian modes, and the generalized coherent states that form a general family to comprise the Hermite-Gaussian and Laguerre-Gaussian mode families as special cases. [1-4] Since the paraxial wave equation of laser cavity can be exactly mapped on the time-dependent two-dimensional quantum harmonic oscillator[5-6], the analogous study of the formation and variation of structured beams make it possible to deeply understand the nature of matter waves.

The development of structured beams related to optical angular momentum[7-10], singular optics[11-13], and optical vortices[14-16] has become popular topics in recent years. The researches not only pave the way for the applications of microparticles manipulation in optical tweezers[17-19] and encoding of information[20-23] but also visualize the intriguing nature of light.[24] For this reason, generation of various structured beams plays an important role to realize the ideas of applications and provides comprehensive insights into wave nature.

In this work, we employ a large-Fresnel-number laser system to demonstrate the exotic three-dimensional (3D) optical coherent waves localized on Lissajous and trochoidal parametric surfaces with Lissajous and trochoidal transverse patterns. The coherent structured beams are verified to be composed of degenerate Hermite-Gaussian and Laguerre-Gaussian modes with different longitudinal indices resulted from longitudinal-transverse coupling in degenerate cavities. Furthermore, we make use of cylindrical lenses to transform the Lissajous structured beams superposed of degenerate Hermite-Gaussian modes into the composition of degenerate Laguerre-Gaussian modes. These degenerate Laguerre-Gaussian modes form the intriguing trochoidal structured beam possessing optical orbital angular momentum. The experimental structured beams are stable and reproducible, and there is a good agreement between numerical and experimental results.

2. Experimental observation and coherent-state representation of Lissajous parametric surfaces

Recently, a diode-pumped microchip laser has been employed to perform the analogous investigation of quantum-classical correspondence and pattern formation.[25-27] In this experiment, the laser system is a diode-pumped Nd:YVO_4

Complex Light and Optical Forces IV, edited by Enrique J. Galvez, David L. Andrews, Jesper Glückstad,
Proc. of SPIE Vol. 7613, 761302 · © 2010 SPIE · CCC code: 0277-786X/10/$18 · doi: 10.1117/12.840804

microchip laser and the resonator configuration is depicted in Fig. 1. The laser gain medium was a a-cut 2.0-at. % Nd:YVO_4 crystal with a length of 2 mm and transverse cross section of 5×5 mm^2. One side of the crystal was coated for partial reflection at 1064nm. The radius of curvature of the cavity mirror is R=10 mm and its reflectivity is 99% at 1064nm. The pump source was an 809 nm fibercoupled laser diode with a core diameter of 100 μm, a numerical aperture of 0.16, and a maximum output power of 1W. A focusing lens was used to reimage the pump beam into the laser crystal. We use off-axis pump scheme to generate 3D coherent waves, and the threshold power of the lasing mode is less than 0.5W. To measure the transverse patterns under propagation, a microscope objective lens was employed to reimage the tomographic transverse patterns onto a CCD camera.

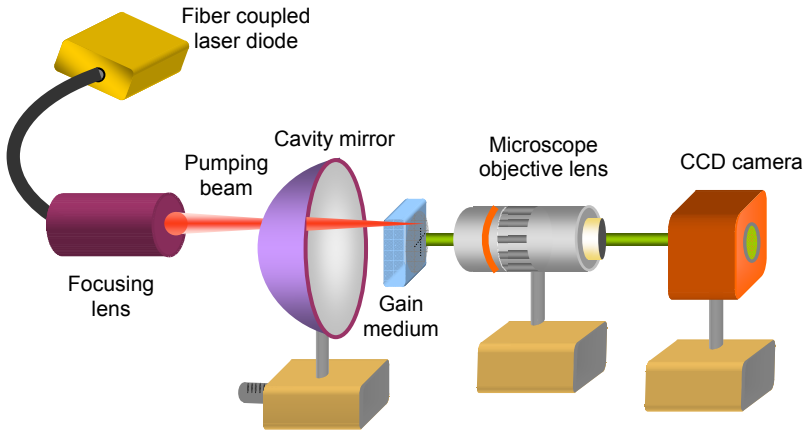

Figure 1. Experimental setup for the generation of structured beams in large-Fresnel number degenerate cavity with off-axis pumping scheme.

For an empty plane-concave resonator consisting of spherical mirror with radius of curvature R and cavity length L, the bare ratio between the transverse and longitudinal mode spacing is given by $\Omega = \Delta f_T / \Delta f_L = (1/\pi)\cos^{-1}\sqrt{1-L/R}$. The bare ratio can be changed in the range between 0 to $1/2$ by varying the cavity length L for a given R in the half-spherical cavity. It has been evidenced[27-28] that when the ratio $\Delta f_T / \Delta f_L$. is close to a simple fractional, the longitudinal-transverse coupling usually leads to the frequency locking among different transverse modes with the help of different longitudinal orders and forms 3D coherent waves localized on the parametric surfaces with Lissajous transverse patterns. The wave functions of the Hermite-Gaussian modes for the paraxial wave equation in the spherical laser resonator can be written as

$$\Phi_{n,m,l}^{(HG)}(x,y,z) = \frac{1}{\sqrt{2^{n+m-1}\pi\, n!\, m!}}\frac{1}{w(z)}H_n\left(\frac{\sqrt{2}x}{w(z)}\right)H_m\left(\frac{\sqrt{2}y}{w(z)}\right)$$
$$\times\exp\left[-\frac{x^2+y^2}{w(z)^2}\right]\exp\left\{-ik_{n,m,l}\,z\left[1+\frac{x^2+y^2}{2(z^2+z_R^2)}\right]\right\}\exp\left[i(n+m+1)\theta_G(z)\right], \quad (1)$$

where $w(z) = w_0\sqrt{1+(z/z_R)^2}$, w_0 is the beam radius at the waist, $z_R = \sqrt{L(R-L)}$ is the Rayleigh range, $k_{n,m,l}$ is the wave number, $H_m(.)$ is a Hermite polynomial of order m, and $\theta_G(z) = \tan^{-1}(z/z_R)$ is the Gouy phase. In terms of the cavity length L, the wave number $k_{n,m,l}$ is given by $k_{n,m,l}L = \pi\left[l+(n+m)(\Delta f_T/\Delta f_L)\right]$. From the longitudinal-transverse coupling, the 3D coherent optical waves can be expressed as

$$\Psi_{n_0,m_0}^{p,q}(x,y,z;\phi_0)=\sum_{k=-M}^{M} C_{M,k}\, e^{i k \phi_0}\, \Phi_{n_0+pk,m_0+qk,l_0+sk}^{(HG)}(x,y,z) \quad , \tag{2}$$

where $C_{M,k}=2^{-M}\begin{pmatrix}2M\\M+k\end{pmatrix}^{1/2}$ is the weighting coefficient, ϕ_0 is the relative phase between various Hermite-Gaussian modes $\Phi_{n,m,l}^{(HG)}(x,y,z)$ at $z=0$, the indices obey the equation $s+(p+q)(P/Q)=0$ to form a family of frequency degenerate states. The combination of degenerate states forms the stationary coherent wave to connect the relation between wave optics and geometric optics. Figure 2(a) depicts several numerical Hermite-Gaussian modes corresponding to Eq. (1) with different transverse orders. For each Hermite-Gaussian mode, the intensity is invariant under propagation because of the same Gouy phase. Figure 2(b)-(d) show the intensity of the numerical coherent waves corresponding to Eq. (2) with $\Omega=1/2$, $(p,q)=(4,-2)$, $(n_0,m_0)=(48,16)$, $M=2$, and $\phi_0=0$ at different propagation position. The components of the coherent waves are shown in Fig. 2(a). The superposition of Hermite-Gaussian modes according to the rule of longitudinal-transverse coupling leads to the localization of transverse patterns, and the intensity is dependent of propagation position because of the different contribution of Gouy phases from different transverse orders.

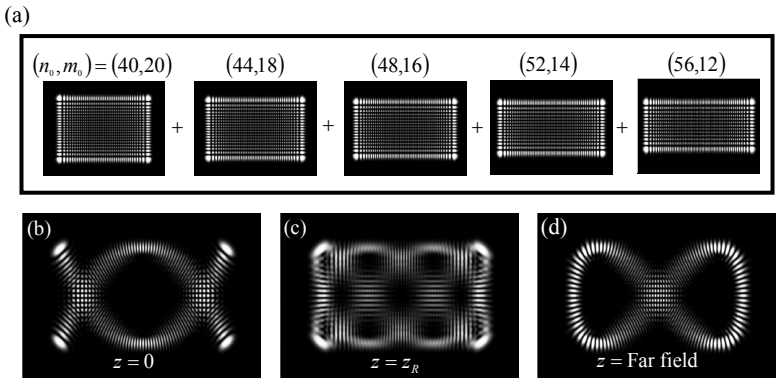

Figure 2. (a) Numerical Hermite-Gaussian modes with different transverse orders. (b)-(d) Superposition of Hermite-Gaussian modes shown in (a) corresponding to Eq. (2) with $\Omega=1/2$, $(p,q)=(4,-2)$, $(n_0,m_0)=(48,16)$, $M=2$, and $\phi_0=0$ at different propagation position.

The experimental optical waves can be generated by use of the large-Fresnel number degenerate cavity with off-axis pumping scheme shown in Fig. 1. Figure 3 depicts the 3D tomography of experimental optical waves with $\Omega=1/2$, $(p,q)=(4,-2)$ under propagation. The experimental results are in good agreement with theoretical results in Fig. 2 for the wave from beam waist to far-field region. The intensity of optical wave inside the cavity is also shown in Fig. 3 as the position of bright pumping spot, and the phase variation of the optical wave from beam waist inside and outside the cavity is the same. It is worthy to mention that there is unlimited number of coherent waves with different (p,q) of the same degenerate cavity as following the degenerate rule. In reality, the numbers of optical waves generated from the same degenerate cavity depend on the parameters of experimental setup such as reflectivity of cavity mirrors. Figure 4 shows the far-field experimental optical waves of degenerate cavity $\Omega=1/4$ around the actual cavity length of 5 mm. Each optical wave in Fig. 4 holds about 30 μm when adjusting the cavity length from 4.7 mm. The optical waves show that the cavity length is longer, the index p is smaller and the transverse index (p,q) is symmetric on the cavity length.

There are twenty optical waves exist around the degenerate cavity $\Omega = 1/4$. These optical waves with transverse Lissajous localization are propagation-variant and form intriguing parametric surfaces in three dimension.

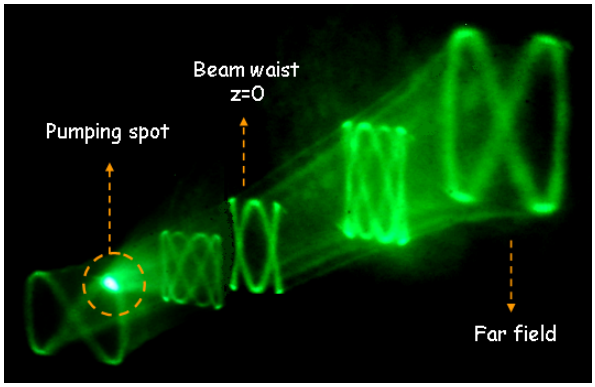

Figure 3. Three-dimensional tomography of experimental optical waves with $\Omega = 1/2$, $(p,q) = (4,-2)$ under propagation.

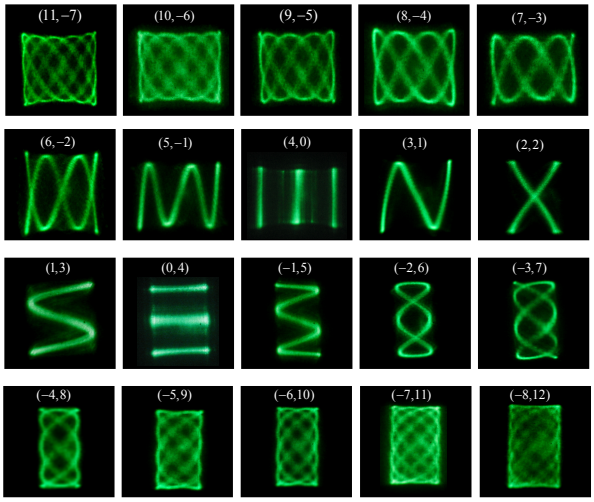

Figure 4. Far-field experimental optical waves of degenerate cavity $\Omega = 1/4$ around the actual cavity length of 5 mm. The index $(11,-7)$ is corresponding to the shortest cavity length, and the index $(-8,12)$ is corresponding to the longest cavity length.

3. Experimental observation and coherent-state representation of superposition of degenerate Laguerre-Gaussian modes

In addition to Hermite-Gaussian modes, the Laguerre-Gaussian modes are also the eigenstates of spherical cavity. The continuous transition from Hermite-Gaussian mode to Laguerre-Gaussian mode has been analytically verified with the generalized coherent states[4]. The Laguerre-Gaussian mode can be decomposed into a sum of Hermite-Gaussian modes as

$$\Phi^{(LG)}_{\tilde{n},\tilde{m},l}(x,y,z)=\sum_{u=0}^{2\tilde{n}+\tilde{m}} e^{\,iu\left(\frac{\pi}{2}\right)}\cdot B(\tilde{n},\tilde{m},u)\cdot\Phi^{(HG)}_{2\tilde{n}+\tilde{m}-u,u,l}(x,y,z) \quad , \tag{3}$$

where

$$B(\tilde{n},\tilde{m},u)=\frac{(-1)^u}{\sqrt{2^{2\tilde{n}+\tilde{m}}}}\sum_{v}\frac{(-1)^v\sqrt{(\tilde{n}+\tilde{m})!\,\tilde{n}!\,(2\tilde{n}+\tilde{m}-u)!\,u!}}{v!\,(u-v)!\,(\tilde{n}+\tilde{m}-v)!\,(\tilde{n}+v-u)!} \quad . \tag{4}$$

The relation of the indices between the Hermite-Gaussian modes and Laguerre-Gaussian modes follows $n=\tilde{n}$ and $m=\tilde{n}+|\tilde{m}|$. Figure 5(a) shows several Laguerre-Gaussian modes corresponding to Eq. (3) with different transverse orders. For each Laguerre-Gaussian mode, the intensity is invariant under propagation because of the same Gouy phase. According to the rule of longitudinal-transverse coupling, the 3D coherent optical waves comprise degenerate Laguerre-Gaussian modes can be expressed as

$$\Psi^{\tilde{p},\tilde{q}}_{\tilde{n}_0,\tilde{m}_0}(x,y,z;\phi_0)=\sum_{k=-M}^{M} C_{M,k}\; e^{ik\phi_0}\;\Phi^{(LG)}_{\tilde{n}_0+\tilde{p}k,\tilde{m}_0+\tilde{q}k,l_0+sk}(x,y,z) \quad , \tag{5}$$

where the indices follow the relation of $\tilde{p}=p$ and $\tilde{p}+\tilde{q}=q$. Figure 5(b) depicts the intensity of the numerical coherent wave corresponding to Eq. (5) with $\Omega=1/5$, $(\tilde{p},\tilde{q})=(-1,7)$, $(\tilde{n}_0,\tilde{m}_0)=(16,51)$, $M=2$, and $\phi_0=0$ for near-field pattern. The components of the coherent waves are shown in Fig. 5(a). The superposition of Laguerre-Gaussian modes

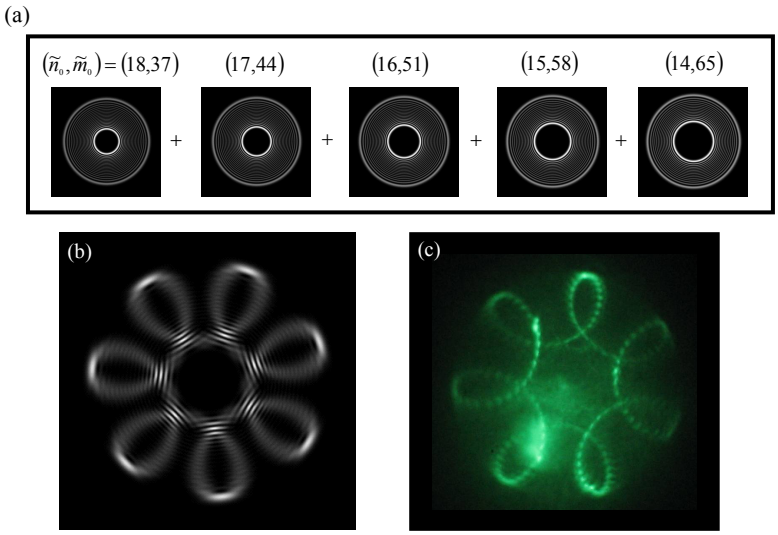

Figure 5. (a) Numerical Laguerre-Gaussian modes with different transverse orders. (b) Superposition of Laguerre-Gaussian modes shown in (a) corresponding to Eq. (5) with $\Omega=1/5$, $(p,q)=(-1,7)$, $(\tilde{n}_0,\tilde{m}_0)=(16,51)$, $M=2$, and $\phi_0=0$ at near field. (c) Experimental result corresponding to (b).

according to the rule of longitudinal-transverse coupling leads to the localization of intriguing trochoidal transverse pattern. To realize the localization of trochoidal transverse modes from laser cavity, we enlarge the off-axis pumping on the gain medium to generate the astigmatism for the transformation of eigenstates from Hermite-Gaussian modes to

Laguerre-Gaussian modes. Figure 5(c) is the experimental result of near-field optical wave related to Fig. 5(b), and there is a good agreement between them. Furthermore, there are several experimental near-field patterns shown in Fig. 6 at different degenerate cavities.

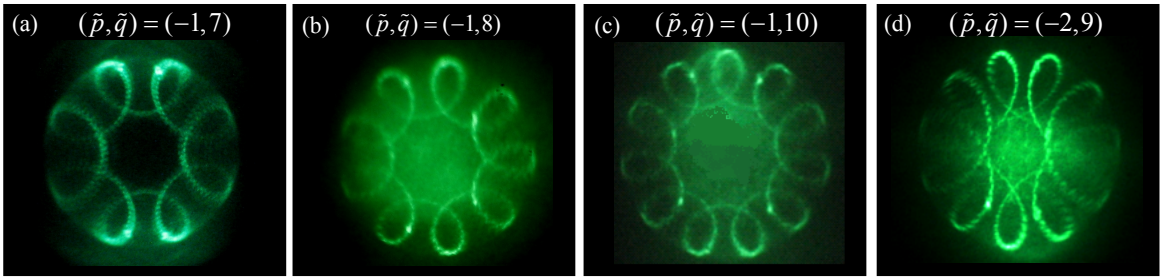

Figure 6. (a) Experimental transverse patterns observed at the beam waist $z=0$ in different cavity lengths: (a) $\Omega=1/6$; (b) $\Omega=1/7$; (c) $\Omega=2/9$; (d) $\Omega=2/7$.

4. Relationship between classical Lissajous and trochoidal parametric surfaces

The state $\Psi^{p,q}_{n_0,m_0}(x,y,z;\phi_0)$ has been verified to have the intensity localized on the Lissajous parametric surface: $x=\mathrm{Re}\left[X(\vartheta,z)\right]$; $y=\mathrm{Re}\left[Y(\vartheta,z)\right]$, where $0\le\vartheta\le 2\pi$, $-\infty\le z\le\infty$, $X(\vartheta,z)=\sqrt{n_0}\,w(z)e^{i[q\vartheta+(\varphi(z)+\phi_0/p)]}$, and $Y(\vartheta,z)=\sqrt{m_0}\,w(z)e^{ip\vartheta}$ [25]. To be precise, the Lissajous parametric surface is formed by the Lissajous curves with the phase factor varying with the position *z*. Using the correspondence between classical canonical transform and quantum unitary transform[28] and the isomorphic relation between SU(2) algebra and SO(3) algebra, we can deduce the Laguerre-Gaussian coherent state $\Psi^{\tilde{p},\tilde{q}}_{\tilde{n}_0,\tilde{m}_0}(x,y,z;\phi_0)$ to be exactly localized on the parametric surface: $x=\mathrm{Re}\left[\tilde{X}(\vartheta,z)\right]$; $y=\mathrm{Re}\left[\tilde{Y}(\vartheta,z)\right]$, where

$$\begin{bmatrix}\tilde{X}(\vartheta,z)\\ \tilde{Y}(\vartheta,z)\end{bmatrix}=\frac{1}{\sqrt{2}}\begin{bmatrix}e^{-i(\pi/4)} & -e^{-i(\pi/4)}\\ e^{i(\pi/4)} & e^{i(\pi/4)}\end{bmatrix}\begin{bmatrix}X(\vartheta,z)\\ Y(\vartheta,z)\end{bmatrix}. \tag{6}$$

It can be easily found that the parametric surfaces in Eq. (6) have the transverse patterns to be the trochoidal curves rotating with the position *z*; therefore, we call these surfaces the trochoidal parametric surfaces. Experimental results reveal that the laser modes are associated with the standing-wave trochoidal coherent states[26]. To be precise, a standing-wave trochoidal coherent state consists of two trochoidal transverse waves rotating in the opposite direction. Figure 7 shows an example to make a comparison between the Lissajous and trochoidal parametric surfaces in the range from $\varphi(z)=-5\pi/2$ to $\varphi(z)=5\pi/2$ with $\phi_0=\pi/2$ for the degenerate cavity $\Omega=1/5$ with $(p,q)=(-1,6)$ and $(\tilde{p},\tilde{q})=(-1,7)$. Different from the eigenstates, Hermite-Gaussian modes and Laguerre-Gaussian modes, the coherent waves generated from the superposition of eigenstates form the exotic parametric surfaces in three dimensions.

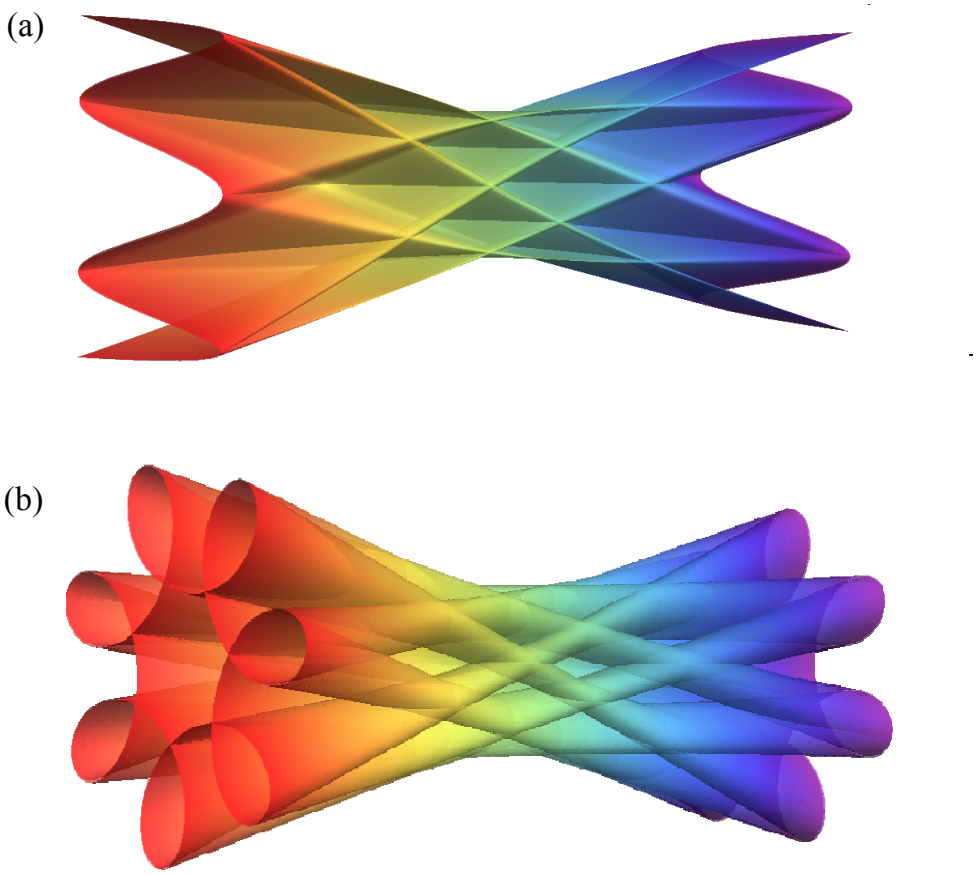

Figure 7. Lissajous (a) and trochoidal (b) parametric surfaces for the 3D coherent waves in the range from $\varphi(z) = -5\pi/2$ to $\varphi(z) = 5\pi/2$ with $\phi_0 = \pi/2$ for the degenerate cavity $\Omega = 1/5$ with $(p,q) = (-1,6)$ and $(\tilde{p},\tilde{q}) = (-1,7)$.

5. Beam transformation from Hermite-Gaussian beam to Laguerre-Gaussian beam

By use of cylindrical lenses, the Hermite-Gaussian beams with transverse index (n,m) in rectangular coordinate can be transformed into Laguerre-Gaussian beams with transverse radial index $\tilde{n}$ and azimuthal index $\tilde{m}$ in cylindrical coordinate. It is worthy to mention that the transformed Laguerre-Gaussian beams which possessing the magnitude of orbital angular momentum $\tilde{m}\hbar$ per photon bring out wide applications for controlling microparticles. Figure 8 depicts the illustration of transformation between Hermite-Gaussian mode and Laguerre-Gaussian mode. Figure 8(a)-(c) represent the simulated high-order Hermite-Gaussian modes with transverse indices $(n,m) = (0,4)$, $(1,4)$, and $(2,4)$. The effect of a pair of cylindrical lenses shown in Fig. 8(e) leads to the transformation of high-order Hermite-Gaussian modes into corresponding high-order Laguerre-Gaussian modes shown in Fig. 8(a')-(c'), respectively. From the point of view, we can expand the transformation relation to analyze more complex structured optical waves resulted from coherent superposition of eigenmodes as Hermite-Gaussian and Laguerre-Gaussian modes. Figure 8(d) and (d') show the experimental results: the optical wave with Lissajous transverse pattern shown in Fig. 8(d) can be transformed to the optical wave with trochoidal transverse pattern in Fig. 8(d') by using of a pair of cylindrical lenses. Importantly, the

transformed optical wave possesses orbital angular momentum, and the magnitude of the orbital angular momentum depends on the order of origin Lissajous wave. We are now studying the details of the interesting transformation between Lissajous and trochoidal transverse patterns.

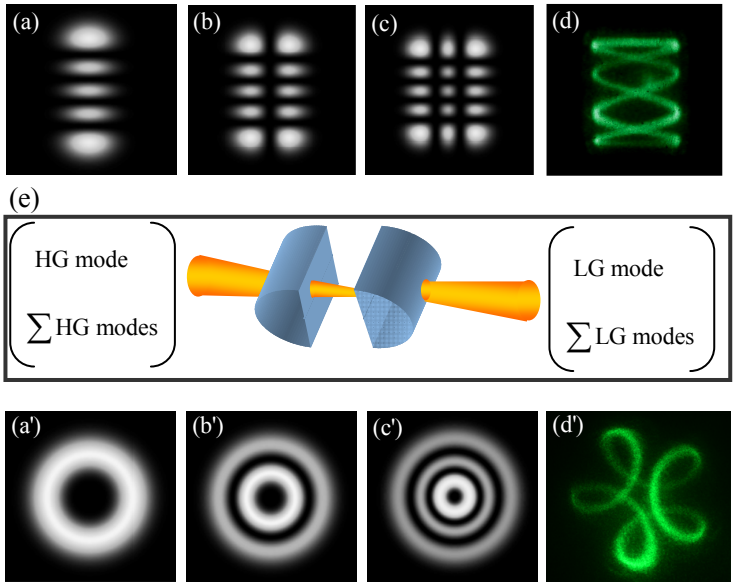

Figure 8. (a)-(c) Numerical results of high-order Hermite-Gaussian modes with transverse indices $(n,m)=(0,4)$, $(1,4)$, and $(2,4)$; (d) Optical wave with Lissajous transverse pattern; (e) Illustration of the effect of cylindrical lenses to transform Hermite-Gaussian modes into Laguerre-Gaussian modes; (a')-(c') Numerical results of Laguerre-Gaussian modes transformed from (a)-(c) with the effect of a pair of cylindrical lenses in (e); (d') Experimental result of transformation from (d) by a pair of cylindrical lenses.

6. Conclusions

In conclusion, the large-Fresnel number laser cavity has been employed to generate various intriguing optical waves localized on Lissajous and trochoidal parametric surfaces. With the theoretical analyses, there is a good agreement between numerical and experimental results. The analogous study of paraxial wave equation and time-dependent two-dimensional quantum harmonic oscillator provides some useful insights into wave nature in mesoscopic scale.

The Lissajous transverse mode comprises degenerate Hermite-Gaussian modes can be transformed into the trochoidal transverse mode possessing orbital angular momentum. The study of manipulation of the intriguing optical modes is proceeding as planned. We expect that the optical orbital angular momentum will be quite large and flexibly manipulated.

REFERENCES

[1] Brambilla, M., Battipede, F., Lugiato, L. A., Penna, V., Prati, F., Tamm, C. and Weiss, C. O., "Transverse laser patterns. I. Phase singularity crystals," Phys. Rev. A 43, 5090-5113 (1991).

[2] Dangoisse, D. , Hennequin, D., Lepers, C., Louvergneaux, E. and Glorieux, P., "Two-dimensional optical lattices in a CO2

laser," Phys. Rev. A 46, 5955-5958 (1992).
[3] Cabrera, E., Calderón, O. G., Melle, S. and Guerra, J. M., "Development of spatial turbulence from boundary-controlled patterns in class-B lasers," Phys. Rev. A 73, 053820 (2006).
[4] Lu, T. H., Chen, Y. F. and Huang, K. F., "Generation of polarization-entangled optical coherent waves and manifestation of vector singularity patterns," Phys. Rev. E 75, 026614 (2007).
[5] van Enk, S. J. and Nienhuis, G., "Eigenfunction description of laser beams and orbital angular momentum of light," Opt. Commun. 94, 147-158 (1992).
[6] Nienhuis, G. and Visser, J., "Angular momentum and vortices in paraxial beams," J. Opt. A: Pure Appl. Opt. 6, 248-250 (2004).
[7] O'Neil, A. T., MacVicar, I., Allen, L. and Padgett, M. J., "Intrinsic and extrinsic nature of the orbital angular momentum of a light beam," Phys. Rev. Lett. 88, 053601 (2002).
[8] Allen, L., Barnett, S. M. and Padgett, M. J., [Optical angular momentum], Institute of Physics Publishing, ISBN 07503 09016) (2003).
[9] Andersen, M. F., Ryu, C., Clade, P., Natarajan, V., Vaziri, A., Helmerson, K. and Phillips, W. D., "Quantized rotation of atomic from photons with orbital angular momentum," Phys. Rev. Lett. 97, 170406 (2006).
[10] Franke-Arnold, S., Allen, L. and Padgett, M. J., "Advances in optical angular momentum," Laser Photonics Rev. 2, 299-313 (2008).
[11] Berry, M. V. and Dennis, M. R., "Knotted and linked phase singularities in monochromatic waves," J. Opt. Soc. Am. B 14, 3054-3065 (1997).
[12] Soskin, M. S. and Vasnetsov, M. V., [Singular optics], in Progress in Optics 42, E. Wolf, 219–276 (2001).
[13] Leach, J., Dennis, M. R., Courtial, J. and Padgett, M. J., "Laser beams: Knotted threads of darkness," Nature 432, 165 (2004).
[14] Rozas, D., Law, C. T. and Swartzlander, Jr., G. A., "Propagation dynamics of optical vortices," J. Opt. Soc. Am. B 14, 3054-3065 (1997).
[15] Izdebskaya, Y., Fadeyeva, T., Shvedov, V. and Volyar, A., "Vortex-bearing array of singular beams with very high orbital angular momentum," Opt. Lett. 31, 2523-2525 (2006).
[16] Baumann, S. M., Kalb, D. M., MacMillan, L. H. and Galvez, E. J., "Propagation dynamics of optical vortices due to Gouy phase," Opt. Express 17 9818-9827 (2009).
[17] Gahagan, K. T. and Swartzlander, Jr., G. A., "Optical vortex trapping of particles," Opt. Lett. 21, 827-829 (1996).
[18] Simpson, N. B., Dholakia, K., Allen, L. and Padgett, M. J., "The mechanical equivalence of the spin and orbital angular momentum of light: an optical spanner," Opt. Lett. 22, 52-54 (1997).
[19] Adachi, H., Akahoshi, S. and Miyakawa, K., "Orbital motion of spherical microparticles trapped in diffraction patterns of circularly polarized light," Phys. Rev. A 75, 063409 (2007).
[20] Gibson, G., Courtial, J., Padgett, M. J., Vasnetsov, M., Pas'ko, V., Barnett, S. M. and Franke-Arnold, S., "Free-space information transfer using light beams carrying orbital angular momentum," Opt. Express 12, 5448-5456 (2004).
[21] Garcia-Escartin, J. C. and Chamorro-Posada, P., "Quantum multiplexing with the orbital angular momentum of light," Phys. Rev. A 78, 062320 (2008).
[22] Nagali, E., Sciarrino, F., Martini, F., Marrucci, L., Piccirillo, B., Karimi, E. and Santamato, E., "Quantum information transfer from spin to orbital angular momentum of photons," Phys. Rev. Lett. 103, 013601 (2009).
[23] Chen, L. and She, W., "Encoding orbital angular momentum onto multiple spin states based on a Huffman tree," New J. Phys. 11 103002 (2009).
[24] Andrews, D. L., [Structured light and its applications: An Introduction to Phase-Structured Beams and Nanoscale Optical Forces], Academic Press-Elsevier, Burlington, (2008).
[25] Chen, Y. F., Lu, T. H., Su, K. W. and Huang, K. F., "Devil's staircase in three-dimensional coherent waves localized on Lissajous parametric surfaces," Phys. Rev. Letts. 96, 213902 (2006).
[26] Lu, T. H., Lin, Y. C., Chen, Y. F. and Huang, K. F., "Three-dimensional coherent optical waves localized on trochoidal parametric surfaces," Phys. Rev. Letts. 101, 233901 (2008).
[27] Lu, T. H., Lin, Y. C., Chen, Y. F. and Huang, K. F., "Observation and analysis of coherent optical waves emitted from large-Fresnel number degenerate cavities," Opt. Express 17, 3007-3014 (2009).
[28] Dirac, P. A. M., [The Principle of Qunatum Mechanics], Oxford University Press, Oxford, 4th ed. (1958).

Acknowledgments

The authors thank the National Science Council for their financial support of this research under Contract No. NSC-98-2112-M-003-008-MY3.